This is a preprint of the following article, which is available at: http://mdolab.engin.umich.edu
M. Shahabsafa, R. Fakhimi, W. Lei, S. He, L. Zuluaga, J. R. R. A. Martins, T. Terlaky, Truss topology design optimization with guaranteed kinematic stability. *Structural and Multidisciplinary Optimization*, (In press).
The original article may differ from this preprint and is available at:
https://link.springer.com/article/10.1007/s00158-020-02698-x.

Truss topology design and sizing optimization with guaranteed kinematic stability

Mohammad Shahabsafa, Ramin Fakhimi, Weiming Lei, Luis Zuluaga, and Tamás Terlaky
Department of Industrial and Systems Engineering, Lehigh University, Bethlehem, PA

Sicheng He and Joaquim R. R. A. Martins
University of Michigan, Department of Aerospace Engineering, Ann Arbor, MI 48109

Abstract

Kinematic stability is an often overlooked, but crucial aspect when mathematical optimization models are developed for truss topology design and sizing optimization (TTDSO) problems. In this paper, we propose a novel mixed integer linear optimization (MILO) model for the TTDSO problem with discrete cross-sectional areas and Euler buckling constraints. Random perturbations of external forces are used to obtain kinematically stable structures. We prove that, by considering appropriate perturbed external forces, the resulting structure is kinematically stable with probability one. Furthermore, we show that necessary conditions for kinematic stability can be used to speed up the solution of discrete TTDSO problems. Using the proposed TTDSO model, the MILO solver provides optimal or near optimal solutions for trusses with up to 990 bars.

1 Introduction

The truss design problem is an important problem in the field of structural design optimization (Haftka and Gürdal, 2012). In the past, various formulations and solution methodologies for truss design problems have been developed (see, e.g., Arora and Wang, 2005; Rozvany, 2009; Stolpe, 2016). Dorn et al. (1964) considered a ground structure framework for the truss design problem and used numerical optimization to solve the problem. In a ground structure framework, the set of potential bars of a truss structure is given and the optimal cross-sectional areas of the bars are to be determined.

Two objectives are commonly used in truss design problems. A wide range of mathematical models for truss design problems consider the structure's compliance minimization as the objective (Ben-Tal and Bendsøe, 1993; Bendsøe et al., 1994; Stolpe, 2007). In turn, several second-order cone optimization and semi-definite optimization models have been suggested to address compliance minimization for TTDSO problems (Kanno, 2016; Kanno and Fujita, 2018; Ben-Tal and Bendsøe, 1993). Kanno (2018), for example, proposed a robust mixed integer semi-definite optimization (MISDO) model for the minimum-compliance truss topology design and sizing optimization problem with uncertainty of the external loads and developed a heuristic method to solve the proposed MISDO model.

Another frequently used objective in truss design problems is weight minimization (Stolpe and Svanberg, 2004; Stolpe, 2004; Van Mellaert et al., 2015; Shahabsafa et al., 2018). Minimizing the structure's weight which ultimately reduces the fuel burn rate is commonly considered in aerospace engineering design problems (Brooks et al., 2017; Jasa et al., 2018; Chauhan and Martins, 2018; Kennedy, 2016; Aage et al., 2017).

Besides the objective function, we can also categorize the problems by the design variable types. There are two types of truss design problems: continuous and discrete design problems. In continuous problems, all the design variables including the cross-sectional areas of the bars are continuous; while discrete problems involve discrete design variables. Zegard and Paulino (2014, 2015) have developed a *ground structure method* to solve large-scale truss topology optimization problems. They focus on continuous truss topology optimization problems and do not take into account Euler buckling constraints. Further, kinematic stability is not considered in their mathematical optimization model. The resulting structure is instead post-processed to enforce kinematic stability.

Discrete problems have three major categories: truss topology design (TTD), truss sizing optimization (TSO), and truss topology design and sizing optimization (TTDSO). We focus on MILO modeling approaches, which lead to a global optimal solution of the discrete truss design problems. Due to the rapid improvement of MILO solution methodologies, we can solve large-scale problems to optimality in a reasonable time as demonstrated in Section 5. Stolpe (2007) suggested a MILO model for compliance minimization of a TTD problem. In TSO, the topology is given and the bar cross-sectional areas of the optimal bars are to be determined. Van Mellaert et al. (2015) proposed a MILO model for TSO problems considering resistance and joint geometry constraints. Shahabsafa et al. (2018) presented several MILO models for TSO problems considering Hooke's law, yield stress and Euler buckling constraints. However, in TTDSO, the topology and sizing of a truss are simultaneously considered. Stolpe (2015) considered a mixed integer nonlinear optimization model for the TTDSO problem in which the structure maximum compliance is considered as a constraint of the model. Stolpe (2016) presented a comprehensive survey of discrete truss design problems.

A variety of solution methodologies are used to solve TTDSO problems. It should be noted that that we do not consider heuristic and meta-heuristic methods that are frequently used to solve the TTDSO problems (see, e.g., Stolpe (2016)). Nor we consider SIMP-type methods (Bendsøe, 1989; Zhou and Rozvany, 1991), which are used

to solve finite element based structures where each element either exists or does not. Our goal is to efficiently obtain global optimal solutions for TTDSO problems with a finite number of possible cross-sectional areas. Thus, we focus on global optimization approaches for the complex TTDSO problem.

It is assumed in TSO problems that the given ground structure is kinematically stable; while kinematic stability of the solution in TTD and TTDSO needs to be enforced. Enforcing kinematic stability in a truss structure makes the problem significantly harder to solve and thus, it is often overlooked when tackling truss design problems. It should be noted that, in the article, we have not taken the inertia load into consideration, and thus, we focus on static stability.

One way to enforce the kinematic stability of a truss structure is to develop a semidefinite optimization (SDO) model and add a constraint on the minimum eigenvalue of the stiffness matrix to the model. Achtziger and Kočvara (2007) developed a bilinear SDO model for the discrete TTDSO problem with the objective of maximizing the smallest natural frequency of the structure. They proposed an algorithm for finding a high quality solution. Their resulting structures are kinematically stable. Hashimoto and Kanno (2015) proposed a SDO model for the continuous TTDSO problems and by imposing a constraint on the minimum eigenvalue of the stiffness matrix, they proved that the resulting structure will be kinematically stable. However, they did not consider discrete cross-sectional areas. Note that only small-scaled MISDO problems can currently be solved to global optimality (Gally et al., 2018).

An alternative way is to enforce kinematic stability in a MILO framework which is significantly easier to solve than attempting to solve MISDO problems. Faustino et al. (2006) proposed a MILO model for the TTDSO problem. They considered structure kinematic stability by using Grubler's criterion (Ghosh and Mallik, 2002), which is a necessary but not sufficient condition for having a kinematically stable structure. Faustino et al. (2006), additionally, proposed a perturbation of the external forces to obtain kinematically stable structures, and without formal statement, they argued intuitively that the perturbation should result in a kinematically stable structure. However, they did not rigorously prove that the perturbation guarantees kinematic stability of the structure. Kanno and Guo (2010) considered an iterative external force perturbation method to obtain a kinematically stable structure for the TTDSO problem with discrete cross-sectional areas. However, their method does not guarantee kinematic stability of the structure. Mela (2014) developed a MILO model for minimum weight discrete TTDSO problems considering Euler buckling and displacement constraints. Mela (2014) also considered the kinematic stability of the structure and the issue of overlapping bars in TTDSO problems. To enforce kinematic stability of the structures, Mela (2014) used the external force perturbation approach which was originally proposed by Faustino et al. (2006). Mela (2014) observed that the perturbation provided stable structures for all the cases he considered, but did not prove that the approach always provides a kinematically stable structure.

Guaranteed kinematic stability of the structure is a fundamentally important problem that has remained an open question in the MILO modeling framework. In this paper, we focus on the minimum-weight discrete TTDSO problem. We propose a novel MILO model for discrete TTDSO problems. Our model considers force balance equa-

tions, Hooke's law, yield stress, Euler buckling constraints, and bounds on the nodal displacements. We also propose a modeling approach that enables us to formally prove the kinematic stability of the structure, and we rigorously prove that the solution of our novel model is kinematically stable. Furthermore, we show that the necessary conditions for kinematic stability can be used to speed-up the solution of TTDSO problems.

The paper is structured as follows. In Section 2, we provide a comprehensive review of the TTDSO problem. In Section 3, we propose a novel mathematical model for the discrete TTDSO problem. In Section 4, we propose a method to enforce the kinematic stability of the structure and prove that, with probability one, the resulting optimal structure is kinematically stable. In Section 5, we present a family of Michell structure problems as our test-set library, and we demonstrate that the proposed mathematical model can be solved significantly faster than other proposed discrete TTDSO models. Finally, our conclusions are presented in Section 6.

2 Problem description

A truss design problem is concerned with the optimal selection of the geometry, topology, and sizing of a truss structure (Haftka and Gürdal, 2012). In this article, we focus on topology and sizing optimization of a truss. Consider a truss structure in a d-dimensional space ($d = 2, 3$). Let m and n denote the number of the bars and the degrees of freedom of the ground structure, respectively. For ease of presentation, we assume that each node of the ground structure is either fixed in all directions or pinned. Let $\mathcal{I} = \{1, \dots, m\}$ be the index set of the bars of the ground structure and let $\mathcal{J}$ denote the index set of the pinned nodes of the ground structure. Vector $x \in \mathbb{R}^m_+$ denotes the cross-sectional areas of the bars, where $\mathbb{R}^m_+$ is the set of m-dimensional non-negative vectors. A truss structure is specified when the bars and their cross-sectional areas are determined. As a result, the cross-sectional areas are the main design variables of the problem.

Let $R \in \mathbb{R}^{n\times m}$ be the topology matrix of the truss. Vector $r_i \in \mathbb{R}^n$, for $i \in \mathcal{I}$, is the i-th column of the matrix R and is equal to the topology of the i-th bar (Haftka and Gürdal, 2012). The force balance equations on the nodes of the truss are given by

$$Rq = f, \tag{1}$$

where $q \in \mathbb{R}^m$ is the vector of the internal forces acting on the bars, and $f \in \mathbb{R}^n$ is the vector of the external forces exerted on the nodes. Stress on bar i, for $i \in \mathcal{I}$, is defined as

$$\sigma_i = \begin{cases} \dfrac{q_i}{x_i}, & \text{if } x_i > 0, \\ 0, & \text{otherwise.} \end{cases} \tag{2}$$

The nodal displacements and the elongation of the bars are denoted by $u \in \mathbb{R}^n$ and $\Delta l \in \mathbb{R}^m$. The relationship between the nodal displacement and the elongation of the

bars is as follows:

$$\Delta l = R^T u. \tag{3}$$

We define $\lambda_i = E_i/l_i$, for $i \in \mathcal{I}$, where E_i and l_i are the Young's modulus and the length of bar $i \in \mathcal{I}$. We consider Hooke's law, which is enforced by considering constraints (1), (2), and (3) along with the following set of constraints (Zienkiewicz and Taylor, 2005):

$$\sigma_i = \lambda_i \Delta l_i, \ i \in \mathcal{I}. \tag{4}$$

From equations (1), (2), (3), and (4), it follows that

$$K(x)u = f,$$

where $K(x) = \sum_{i=1}^{m} \lambda_i x_i r_i r_i^T$ is the stiffness matrix of the structure, and r_i, for $i \in \mathcal{I}$, is the i-th column of the topology matrix R.

Let $\sigma^{\min} \in \mathbb{R}^m$ and $\sigma^{\max} \in \mathbb{R}^m$ be the lower and upper bounds on the stress of the bars, where $\sigma^{\min} < 0 < \sigma^{\max}$. The stress on bars should satisfy the following constraints

$$\sigma^{\min} \leq \sigma \leq \sigma^{\max}.$$

We assume that bars' cross-sections are circular. Thus, by letting $\gamma_i = \pi E_i / 4 l_i^2$, for $i \in \mathcal{I}$, the Euler buckling constraints can be formulated as

$$\sigma_i + \gamma_i x_i \geq 0, \ i \in \mathcal{I}, \ x_i \neq 0. \tag{5}$$

For a discussion on the value of γ_i, $i \in \mathcal{I}$, for more general cross-sectional areas of bars see, e.g., Shahabsafa et al. (2018). Note that we do not consider global buckling of the structure. Instead, we follow the typical modeling choice of imposing local buckling constraints (see, e.g., Stolpe, 2004; Mela, 2014; Bons and Martins, 2020; Kennedy and Martins, 2014)

Let $\mathcal{L}$ denote the index set of the coordinates of the pinned nodes of the ground structure. Note that $|\mathcal{L}| = |\mathcal{J}|d = n$. The nodal displacement bound constraints are given by

$$u_\ell^{\min} \leq u_\ell \leq u_\ell^{\max}, \ \ell \in \mathcal{L}. \tag{6}$$

3 Mathematical optimization model

In this section, we propose a mathematical optimization model for the discrete TTDSO problem, where bars take zero or discrete-valued cross-sectional areas. In other words, in the TTDSO, we allow the bars to vanish in the final structure. This model is an extension of the model proposed by Shahabsafa et al. (2018) for discrete truss sizing optimization problems.

Define $\mathcal{S}$ as the set of candidate nonzero cross-sectional areas of bars:

$$\mathcal{S} = \{s_1, s_2, \ldots, s_v\},$$

where $0 < s_1 < s_2 < \ldots < s_v$ and v is the cardinality of set $\mathcal{S}$. Without loss of generality, we may assume that the number of candidate sizes is the same for all the bars. Furthermore, for ease of presentation, we assume that all the bars have the same set $\mathcal{S}$ of potential cross-sectional areas. We use $\mathcal{K} = \{1, \ldots, v\}$ to denote the set of indices corresponding to the discrete set $\mathcal{S}$. The cross-sectional area of bar i, for $i \in \mathcal{I}$, takes values from the set $\{0\} \cup \mathcal{S}$ in the discrete TTDSO problem. We define a binary decision variable y_i, for $i \in \mathcal{I}$, as

$$y_i = \begin{cases} 1, & \text{if } x_i > 0, \\ 0, & \text{otherwise.} \end{cases} \tag{7}$$

If $y_i = 1$, then bar i gets a nonzero cross-sectional area, and if $y_i = 0$, then bar i has a zero cross-sectional area and disappears from the structure. Let σ_{ik}, for $i \in \mathcal{I}$ and $k \in \mathcal{K}$, be defined as

$$\sigma_{ik} = \begin{cases} \lambda_i \Delta l_i, & \text{if } x_i = s_k, \\ 0, & \text{otherwise.} \end{cases} \tag{8}$$

Variable σ_{ik} represents the stress on bar i if its cross-sectional area is equal to s_k; otherwise, σ_{ik} is zero. Thus, we have that

$$\sigma_i = \sum_{k \in \mathcal{K}} \sigma_{ik}, \quad i \in \mathcal{I}.$$

Additionally, we define σ_i^{d} as

$$\sigma_i^{\mathrm{d}} = \begin{cases} \lambda_i \Delta l_i, & \text{if } x_i = 0, \\ 0, & \text{otherwise.} \end{cases} \tag{9}$$

Variable σ_i^{d}, for $i \in \mathcal{I}$, is a dummy variable that is equal to zero if bar i takes a nonzero cross-sectional area. However, if $x_i = 0$, then σ_i^{d} takes a nonzero value. Then, from equations (8) and (9), we have that

$$\lambda_i \Delta l_i = \sum_{k \in \mathcal{K}} \sigma_{ik} + \sigma_i^{\mathrm{d}}, i \in \mathcal{I}. \tag{10}$$

Sved and Ginos (1968) showed that when a bar has a zero cross-sectional area, the Euler buckling and yield stress constraints must become inactive for that bar. As in equation (10), all variables σ_{ik}, for $k \in \mathcal{K}$, can be equal to zero by introducing variable σ_i^{d}. Thus, introducing dummy stress variables σ_i^{d}, for $i \in \mathcal{I}$, ensures that the Euler buckling and yield stress constraints become inactive if the cross-sectional area of a bar is zero.

To enforce that $x_i \in \{0\} \cup \mathcal{S}$, for all $i \in \mathcal{I}$, we use the *incremental model* proposed by Shahabsafa et al. (2018, Section 2.2). Let $\bar{\mathcal{K}} = \{1, \ldots, v-1\}$ and $\delta_k = s_{k+1} - s_k$ for

$k \in \bar{\mathcal{K}}$. In the incremental model of the discrete TTDSO problem, the cross-sectional areas of the bars are given as:

$$\begin{array}{lll} x_i = s_1 y_i + \sum_{k \in \bar{\mathcal{K}}} \delta_k z_{ik}, & i \in \mathcal{I}, & \\ y_i \geq z_{i1}, & i \in \mathcal{I}, & \\ z_{i,k-1} \geq z_{ik}, & i \in \mathcal{I}, \ k \in \bar{\mathcal{K}} \setminus \{1\}, & \\ y_i \in \{0,1\}, & i \in \mathcal{I}, & \\ z_{ik} \in \{0,1\}, & i \in \mathcal{I}, \ k \in \bar{\mathcal{K}}. & \end{array} \tag{11}$$

If $y_i = 1$ and $z_{i1} = 0$, then $x_i = s_1$. If $z_{i,k-1} = 1$ and $z_{ik} = 0$, then $x_i = s_k$. If $z_{i,v-1} = 1$, then $x_i = s_v$. It should be noted that for a truss structure including m bars and v available discrete values for cross-sectional areas, there are $m \times v$ binary variables.

The following set of constraints are needed to enforce yield stress and Euler buckling constraints

$$\begin{array}{lll} \max\left(-\gamma_i s_1, \sigma_i^{\min}\right)(y_i - z_{i1}) \leq \sigma_{i1} \leq \sigma_i^{\max}(y_i - z_{i1}), & & i \in \mathcal{I}, \\ \max\left(-\gamma_i s_k, \sigma_i^{\min}\right)(z_{i,k-1} - z_{ik}) \leq \sigma_{ik} \leq \sigma_i^{\max}(z_{i,k-1} - z_{ik}), & & \\ & k \in \bar{\mathcal{K}} \setminus \{1\}, & i \in \mathcal{I}, \\ \max\left(-\gamma_i s_v, \sigma_i^{\min}\right) z_{i,v-1} \leq \sigma_{iv} \leq \sigma_i^{\max} z_{i,v-1}, & & i \in \mathcal{I}, \\ (1 - y_i)\underline{\sigma}_i^{\mathrm{d}} \leq \sigma_i^{\mathrm{d}} \leq (1 - y_i)\overline{\sigma}_i^{\mathrm{d}}, & & i \in \mathcal{I}. \end{array} \tag{12}$$

From constraints (12), it follows that if $y_i = 0$, then $\sigma_{ik} = 0$, for all $k \in \mathcal{K}$, and $\underline{\sigma}_i^{\mathrm{d}} \leq \sigma_i^{\mathrm{d}} \leq \overline{\sigma}_i^{\mathrm{d}}$, where

$$\begin{aligned} \underline{\sigma}_i^{\mathrm{d}} &= \lambda_i \left(\sum_{\ell | r_{i\ell} < 0} r_{i\ell} u_\ell^{\max} + \sum_{\ell | r_{i\ell} > 0} r_{i\ell} u_\ell^{\min} \right), \\ \overline{\sigma}_i^{\mathrm{d}} &= \lambda_i \left(\sum_{\ell | r_{i\ell} < 0} r_{i\ell} u_\ell^{\min} + \sum_{\ell | r_{i\ell} > 0} r_{i\ell} u_\ell^{\max} \right). \end{aligned} \tag{13}$$

Equation (13) is obtained from (3), (4), and (6). If $y_i = 1$, which implies that $x_i > 0$, then $\sigma_i^{\mathrm{d}} = 0$. In addition, if $z_{i,\bar{k}-1} = 1$ and $z_{i\bar{k}} = 0$, then $\sigma_{ik} = 0$, for all $k \neq \bar{k}$ and $\max(-\gamma_i s_{\bar{k}}, \sigma_i^{\min}) \leq \sigma_{i\bar{k}} \leq \sigma_i^{\max}$.

Next, we propose sets of constraints to avoid crossing bars. Let set $\mathcal{A}^{\mathrm{p}}$ be the collection of pairs of bars that cross each other. The following set of constraints, which are presented by Mela (2014), prevents crossing bars:

$$y_{i_1} + y_{i_2} \leq 1 \qquad \forall (i_1, i_2) \in \mathcal{A}^{\mathrm{p}} \tag{14}$$

The number of constraints (14) increases rapidly as the ground structure becomes more dense. Let $\mathcal{A}_i$, for $i \in \mathcal{I}$, be the set of the bars that cross bar i. Following is an alternative formulation of the bar-crossing elimination constraints:

$$\sum_{\bar{i} \in \mathcal{A}_i} y_{\bar{i}} \leq |\mathcal{A}_i|(1 - y_i) \qquad i \in \mathcal{I}. \tag{15}$$

Note that we have at most m constraints in (15) in contrast to (14) where the number of constraints increases quadratically as m grows. Adding either constraints (14) or constraints (15) is sufficient to prevent crossing bars. However, adding both sets helps to provide a tighter formulation which ultimately helps to reduce solution time.

Not only crossing bars, but also overlapping bars need to be avoided in a TTDSO problem.

Definition 3.1 (Overlapping set)**.** An overlapping set is a set of bars such that each pair of the bars from that given set overlap (Mela, 2014).

Definition 3.2 (Maximal overlapping set)**.** A maximal overlapping set is an overlapping set that is not a subset of another overlapping set.

Definition 3.3 (Base element of a maximal overlapping set)**.** The smallest bar of an overlapping set is called the base element of that overlapping set.

To ensure that the truss structure does not have any overlapping bars, it is enough to ensure that from each maximal overlapping set at most one bar is active in the structure. Let $\mathcal{I}^B$ be the index set of all the base elements of the overlapping sets, and let $\mathcal{C}_i$, for $i \in \mathcal{I}^B$, be the maximal overlapping set corresponding to base element i. The following set of constraints ensure that we do not have any overlapping bars in the structure:

$$\sum_{\bar{i} \in \mathcal{C}_i} y_{\bar{i}} \leq 1, \qquad i \in \mathcal{I}^B. \tag{16}$$

Note that we have at most m bar-overlapping elimination constraints (16).

The incremental model for the TTDSO problem is then formulated as follows:

An alternative to model (17) for the discrete TTDSO problem is obtained by considering, instead of the incremental model (11) for the discrete cross-sectional areas, a *basic* choice of binary variables (as in Shahabsafa et al. (2018)). The model is presented in the Appendix.

Let $\mathcal{N}_\ell$, for $\ell \in \mathcal{L}$, be the set of the bars of the ground structure that are connected to the node corresponding to the ℓ-th coordinate of the displacement vector. The following constraints enforce that if no bar is connected to a node, then the displacement of that node is zero:

$$u_\ell^{\min} \sum_{i \in \mathcal{N}_\ell} y_i \leq u_\ell \leq u_\ell^{\max} \sum_{i \in \mathcal{N}_\ell} y_i, \ \ \ell \in \mathcal{L}. \tag{18}$$

Adding constraint (18) to the MILO model (17) increases the solution time of the problem. If constraint (18) is not added, the displacements of the nodes with no bars connected to them may be nonzero. However, the optimal cross-sectional areas of the problem do not change, that is, the optimal structure still satisfies all the constraints of the problem even if constraint (18) is not added. Thus, in what follows, instead of adding constraint (18) to the model, as a post-processing step, we set the displacements of the nodes with no bars connected to them to zero. Model (17) can be extended, as done by Mela (2014), to account for multi-scenario discrete TTDSO problems.

$$
\begin{array}{lllll}
\min & \displaystyle\sum_{i\in\mathcal{I}} \rho l_i x_i, & & & \\
\text{s.t.} & Rq & = & f, & \\
& R^T u & = & \Delta l, & \\
& x_i - s_1 y_i - \displaystyle\sum_{k\in\bar{\mathcal{K}}} \delta_k z_{ik} & = & 0, & i\in\mathcal{I}, \\
& \lambda_i \Delta l_i - \displaystyle\sum_{k\in\mathcal{K}} \sigma_{ik} - \sigma_i^{\mathrm{d}} & = & 0, & i\in\mathcal{I}, \\
& q_i - \displaystyle\sum_{k\in\mathcal{K}} s_k \sigma_{ik} & = & 0, & i\in\mathcal{I}, \\
& \max\left(-\gamma_i s_1, \sigma_i^{\min}\right)(y_i - z_{i1}) & \le & \sigma_{i1} \le \sigma_i^{\max}(y_i - z_{i1}), & i\in\mathcal{I}, \\
& \max\left(-\gamma_i s_k, \sigma_i^{\min}\right)\left(z_{i,k-1} - z_{ik}\right) & \le & \sigma_{ik} \le \sigma_i^{\max}\left(z_{i,k-1} - z_{ik}\right), & i\in\mathcal{I}, k\in\bar{\mathcal{K}}\setminus\{1\}, \\
& \max\left(-\gamma_i s_v, \sigma_i^{\min}\right) z_{i,v-1} & \le & \sigma_{iv} \le \sigma_i^{\max} z_{i,v-1}, & i\in\mathcal{I}, \\
& (1-y_i)\underline{\sigma}_i^{\mathrm{d}} & \le & \sigma_i^{\mathrm{d}} \le (1-y_i)\overline{\sigma}_i^{\mathrm{d}}, & i\in\mathcal{I}, \\
& u_\ell^{\min} & \le & u_\ell \le u_\ell^{\max}, & \ell\in\mathcal{L}, \\
& y_{i_1} + y_{i_2} & \le & 1, & (i_1,i_2)\in\mathcal{A}^{\mathrm{p}}, \\
& \displaystyle\sum_{\bar{i}\in\mathcal{A}_i} y_{\bar{i}} & \le & |\mathcal{A}_i|(1-y_i), & i\in\mathcal{I}, \\
& \displaystyle\sum_{\bar{i}\in\mathcal{C}_i} y_{\bar{i}} & \le & 1, & i\in\mathcal{I}^B, \\
& z_{i1} & \le & y_i, & i\in\mathcal{I}, \\
& z_{ik} & \le & z_{i,k-1}, & i\in\mathcal{I},\ k\in\bar{\mathcal{K}}\setminus\{1\}, \\
& y_i\in\{0,1\}, & & & i\in\mathcal{I}, \\
& z_{ik}\in\{0,1\}, & & & i\in\mathcal{I},\ k\in\bar{\mathcal{K}}.
\end{array}
\tag{17}
$$

Model (17) differs from the model proposed by Mela (2014) in three aspects: first, the model proposed by Mela (2014) introduces a binary variable for each possible cross-sectional area of a bar, but in model (17) binary variables represent the increments in the cross-sectional areas of the bars. Second, in contrast to the model proposed by Mela (2014), we do not need to introduce binary variables for the nodes of the truss structure in model (17). Third, variables σ_i^{d}, for $i \in \mathcal{I}$, are introduced to ensure that yield stress and Euler buckling constraints are not enforced when a bar vanishes from the structure. In Section 5, we demonstrate that model (17) is solved significantly faster than the model proposed by Mela (2014).

4 Kinematic stability of truss structures

In this section, we first state the necessary conditions for a truss structure to be kinematically stable. Then, we propose a modeling methodology which ensures kinematic stability of the structure. While our method is new, it is similar in its spirit to the methods proposed by Faustino et al. (2006) and Mela (2014). Most importantly, we prove that, with probability one, the truss structures obtained by our method are kinematically stable. In what follows, we refer to the truss corresponding to cross-sectional areas given by $x \in \mathbb{R}^m$ as *structure* x. We need the following definitions to present the results.

Definition 4.1 (Active bars)**.** An active bar of structure x is a bar whose cross-sectional area is greater than zero. The index set of the active bars of structure x is denoted by $\mathcal{I}^x$.

Definition 4.2 (Active nodes)**.** An active node in structure x is a pinned node, which is connected to at least one active bar. The index set of the active nodes of structure x is denoted by $\mathcal{J}^x$.

Definition 4.3 (Active coordinates)**.** The set of active coordinates in structure x is the set of the coordinates corresponding to active nodes in structure x. The index set of the active coordinates of structure x is denoted by $\mathcal{L}^x$.

In what follows, vectors and matrices are defined in the reduced space of the active nodes and active bars. Let m^x and n^x denote the number of active bars and the degrees of freedom of active nodes of structure x, respectively, i.e., $m^x = |\mathcal{I}^x|$ and $n^x = |\mathcal{J}^x| \times d$.

Definition 4.4 (Reduced topology matrix)**.** The reduced topology matrix of structure x, denoted by $R^x \in \mathbb{R}^{n^x \times m^x}$, is the submatrix of the topology matrix corresponding to active nodes and active bars.

Definition 4.5 (Reduced stiffness matrix)**.** The reduced stiffness matrix of structure x, denoted by $K^x(x) \in \mathbb{R}^{n^x \times n^x}$, is the submatrix of the stiffness matrix corresponding to the set of active nodes $\mathcal{J}^x$:

$$K^x(x) = \sum_{i \in \mathcal{I}^x} x_i \lambda_i r_i^x \left(r_i^x\right)^T, \tag{19}$$

where $r_i^x \in \mathbb{R}^{n^x}$ is the topology vector corresponding to the i-th bar (i.e. i-th column of topology matrix R^x) in the lower dimensional space of the active nodes of structure x.

The reduced nodal displacements and reduced external force vector of structure x, respectively denoted by u^x and f^x, are the vectors of the nodal displacements and external forces in the lower-dimensional space of the active nodes.

Definition 4.6 (Kinematic stability)**.** A truss structure with cross-sectional area $x \in \mathbb{R}^m$ is kinematically stable if $(R^x)^T u^x = 0$ implies $u^x = 0$ (Hajela and Lin, 1992; Rajasekaran and Sankarasubramanian, 2001).

Remark. Given that matrix $K^x(x)$ is positive semi-definite, the kinematic stability condition of Definition 4.6 is equivalent to each of the following conditions:

- $\text{rank}(R^x) = n^x$
- $\det(K^x(x)) > 0$; hence, $K^x(x)$ is positive definite.

If structure x is not stable, then it is called an unstable structure.

4.1 Necessary conditions for kinematic stability

We first state the necessary conditions for the kinematic stability of a truss structure. Then, we derive a set of constraints based on those necessary conditions that are used to strengthen formulation (17) to reduce the solution time of discrete TTDSO problems. To derive the necessary conditions, we need the following definition:

Definition 4.7 (Orientation vector)**.** The orientation vector of a bar with respect to one of its end nodes is the unit vector, which starts from that node pointing to the other node.

Suppose the coordinate system is specified. The coordinates of the topology vector r_i, for $i \in \mathcal{I}$, corresponding to one of the end nodes of bar i are equal to the negative of the orientation vector of bar i with respect to that end node. The coordinates of the topology vector r_i corresponding to the nodes that are not connected to bar i are zero.

Proposition 1. If a truss structure is stable, for any active node, the orientation vectors connected to that node span $\mathbb{R}^d$.

Proof. Suppose that we have a stable structure x. We prove the result by contradiction. We assume that there exists an active node in the structure whose set of orientation vectors, corresponding to the active bars connected to that node, do not span $\mathbb{R}^d$.

Let $\bar{R} \in \mathbb{R}^{d \times m^x}$ be the sub-matrix formed by taking the rows of matrix R^x corresponding to the degrees of freedom of that node. The nonzero columns of matrix $\bar{R}$ are multiples of the respective orientation vectors of the active bars connected to that node. Since the set of the orientation vectors does not span the space, we have $\text{rank}(\bar{R}) < d$, which implies that matrix R^x is not full row rank. Hence, we conclude that $\text{rank}(R^x) < n^x$. This contradicts the kinematic stability condition, as noted in Remark 4. □ □

Corollary 1. In a two-dimensional space, an active node in a stable structure has to be connected to at least two bars that are not on one line.

Corollary 2. In a three-dimensional space, an active node in a stable structure has to be connected to at least three bars that are not in one plane.

Let the sets $\mathcal{B}_j$ and $\mathcal{B}_j^x$, for $j \in \mathcal{J}$, be the set of bar indices connected to node j in the ground structure and in structure x, respectively. From Proposition 1, we know that the number of active bars connected to a node should be more than or equal to the dimension of the space. The following constraints ensure this necessary condition:

$$y_i d \leq \sum_{h \in \mathcal{B}_j} y_h, \qquad i \in \mathcal{B}_j, j \in \mathcal{J}. \tag{20}$$

Constraints (20) provide a lower bound on the number of the bars that are connected to an active node to assist with the kinematic stability of the structure. It should be noted that constraints on the number of bars connected to a node have already been mentioned in the literature (see, e.g., Ohsaki and Katoh (2005) and Mela (2014)). However, those constraints are not linked to the dimension of the truss.

Definition 4.8 (Maximal non-spanning set)**.** A maximal non-spanning set is a subset of bars that are connected to a node such that:

(i) the set of orientation vectors corresponding to those bars does not span the space,

(ii) if we add to the set any of the bars not in the set that are connected to that node, then the resulting set of orientation vectors span the space.

Let set $\mathcal{Q}_j$ contain all the maximal non-spanning sets corresponding to node j that have at least a cardinality of d. In other words, given any node $j \in \mathcal{J}$, if $\mathcal{B}_j^x = \bar{\mathcal{Q}}_j$ and $\bar{\mathcal{Q}}_j \in \mathcal{Q}_j$, then structure x is not stable. Additionally, if we add any bars from the set $\mathcal{B}_j \setminus \bar{\mathcal{Q}}_j$ to set $\bar{\mathcal{Q}}_j$, then the resulting set of orientation vector spans the space.

From Proposition 1, we know that, for all $\bar{\mathcal{Q}}_j \in \mathcal{Q}_j$, if $\sum_{i \in \bar{\mathcal{Q}}_j} y_i \geq 1$, then we must have $\sum_{i \in \mathcal{B}_j \setminus \bar{\mathcal{Q}}_j} y_i \geq 1$. This condition is enforced by adding the following constraints to the MILO model (17):

$$\sum_{i \in \bar{\mathcal{Q}}_j} y_i \leq |\bar{\mathcal{Q}}_j| \sum_{i \in \mathcal{B}_j \setminus \bar{\mathcal{Q}}_j} y_i, \qquad \bar{\mathcal{Q}}_j \in \mathcal{Q}_j, j \in \mathcal{J}. \tag{21}$$

Figure 1 shows a simple instance in a three-dimensional space where five bars are connected to node j. In that case, set Q_j is defined as:

$$\mathcal{Q}_j = \big\{\{1,2,3,4\},\{1,5,6\}\big\}.$$

It should be noted that in this example set $\mathcal{Q}_j$ contains all the maximal non-spanning sets with at least three bars.

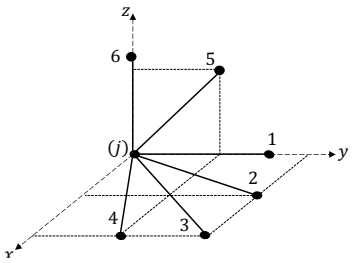

Figure 1: A simple instance of bars connected to a given node j with $d = 3$.

It should be noted that chains are special cases of non-spanning sets; thus by adding constraints (20) and (21), we eliminate chains in the resulting structures. The special case of constraints (21) to eliminate chains was proposed by Mela (2014). Furthermore, hinges (Rozvany, 1996) are special cases of non-spanning sets which are similarly eliminated by constraints (20) and (21).

4.2 Enforcing kinematic stability by external force perturbation

In this section, we propose a method that enforces all the solutions of the discrete TTDSO problem to be kinematically stable structures. The method is similar to the ones proposed by Faustino et al. (2006) and Mela (2014) in that it is based on perturbing the external forces of the truss. Faustino et al. (2006) developed an optimization model based on a perturbation of the external forces and provided the intuition of why their proposed perturbation results in a stable structure. However, they did not specify the characteristics of their proposed random perturbation, which are necessary to ensure kinematically stable trusses. Mela (2014) employed a predefined perturbation, which resembles the perturbation proposed by Faustino et al. (2006). Mela (2014) observed that for all the considered discrete TTDSO problem instances, solving the perturbation model gave a kinematically stable structure. Neither Faustino et al. (2006) nor Mela (2014) proved that their proposed perturbation methodology is guaranteed to eliminate unstable structures. Here, we modify the perturbation methodology proposed by the two articles cited above and rigorously prove that the truss structures obtained by our perturbation method are kinematically stable.

Let $\mathcal{N}_\ell^x$, for $\ell \in \mathcal{L}$, be the set of the bars of structure x with nonzero cross-sectional areas that are connected to the node corresponding to the ℓ-th coordinate of the external force. We assume that the perturbation vector of the external forces, denoted by $p \in \mathbb{R}^n$, is randomly generated as follows:

$$p_\ell = \sum_{i \in \mathcal{N}_\ell} p_{\ell i} y_i, \ \ \ell \in \mathcal{L}, \tag{22}$$

where $p_{\ell i}$, for $\ell \in \mathcal{L}, i \in \mathcal{I}$, are independent random variables with normal distribution with mean zero and variance ϵ^2. Here, ϵ is a small positive real number. If ϵ is a large number, then the perturbation of the external forces may potentially change the optimal solution of the problem. On the other hand, if ϵ is too small, it may lead to numerical instability when solving the problem. It should be noted that, as defined by

equation (22), the random vector p is a function of the decision variable $y \in \mathbb{R}^m$ which enables us to have the perturbation only for the active nodes. Let p^x, for structure $x \in \mathbb{R}^m$, be the reduced perturbation vector in the lower dimensional space of the active nodes.

Proposition 2. The reduced vector p^x, for a given $x \in \mathbb{R}^m$, has an n^x-variate normal distribution.

Proof. Let $x \in \mathbb{R}^m$ be given. From the set of constraints (7), we know that $y_i = 0$, for $i \in \mathcal{I}$, if $x_i = 0$. So we rewrite the perturbation vector p for the given x as

$$p_\ell = \begin{cases} \sum_{i \in \mathcal{N}_\ell^x} p_{\ell i} & \text{if } \ell \in \mathcal{L}^x, \\ 0 & \text{otherwise,} \end{cases} \qquad \ell \in \mathcal{L}. \tag{23}$$

We know that $|\mathcal{L}^x| = n^x$; thus, the perturbation vector p for given x has n^x nonzero coordinates, each of which is a sum of independent normally distributed random variables. Thus, for $\ell \in \mathcal{L}^x$, p_ℓ has a normal distribution with mean zero and variance $|\mathcal{N}_\ell^x|\epsilon^2$. Additionally, the coordinates of the vector p^x are independent of each other. Thus, vector p^x has a multivariate normal distribution. □ □

The perturbed external force $\bar{f} \in \mathbb{R}^n$ is defined as:

$$\bar{f} = f + p. \tag{24}$$

We prove that if the perturbed external force $\bar{f}$ is considered, with probability one, any feasible solution of model (17) is stable. Let $\bar{f}^x$, for structure $x \in \mathbb{R}^m$, be the reduced vector of the perturbed external force $\bar{f}$ in the lower-dimensional space of the active nodes.

Lemma 1. Let structure $x \in \mathbb{R}^m$ be unstable. The probability that the system of equations $K^x(x)u^x = \bar{f}^x$ has a solution for $u^x \in \mathbb{R}^{n^x}$ is zero.

Proof. Let $x \in \mathbb{R}^m$ be given. We compute the probability that the following set of equations holds for structure x:

$$K^x(x)u^x = \bar{f}^x = f^x + p^x. \tag{25}$$

From this set of equations, we have $f^x + p^x \in \text{col}\left(K^x(x)\right)$, where $\text{col}(K^x(x))$ is the column space of matrix $K^x(x)$. Thus, $p^x \in \text{col}\left(K^x(x)\right) - \{f^x\}$.

Since structure x is kinematically unstable, from Definition 4.6, it follows that $\det(K^x(x)) = 0$. Therefore, $\dim\left(\text{col}(K^x(x))\right) < n^x$, and thus,

$$\dim\left(\text{col}(K^x(x)) - \{f^x\}\right) < n^x.$$

From Proposition 2, the random vector p^x has an n^x-variate normal distribution. Therefore, we conclude that the probability that $p^x \in \text{col}\left(K^x(x) - \{f^x\}\right)$, i.e., that p^x is in a subspace with dimension less than n^x, is zero. Thus, the probability that the set of equations (25) holds for an unstable structure is zero. □ □

Corollary 3. The probability that an unstable structure $x \in \mathbb{R}^m$ is feasible for problem (17) with perturbed external force $\bar{f}$ is zero.

Proof. Let $x \in \mathbb{R}^m$ be given. If $K(x)u = \bar{f}$ holds then $K^x(x)u^x = \bar{f}^x$ is satisfied for structure x. Thus, from Lemma 1, we conclude that equation $K(x)u = f$ holds for unstable structure x with probability zero. Additionally, we know that the equation system $K(x)u = f$ is equivalent to the following set of constraints (Shahabsafa et al., 2018):

$$\begin{aligned} Rq &= f, \\ R^T u &= \Delta l, \\ \lambda_i \Delta l_i &= \sigma_i, && i \in \mathcal{I}, \\ q_i &= x_i \sigma_i, && i \in \mathcal{I}. \end{aligned}$$

Thus, the probability that an unstable solution x is feasible for problem (17) is zero. □ □

Theorem 1. The probability that the feasible set of problem (17) with perturbed external force $\bar{f}$, as defined in (24), includes a kinematically unstable structure is zero.

Proof. In the discrete TTDSO problem (17), cross-sectional area x_i, for $i \in \mathcal{I}$, takes values from discrete set $\mathcal{S} \cup \{0\}$. So the set of possible structures in problem (17) is finite, and thus, the set of possible unstable structures is finite. Suppose set $\mathcal{X} = \{x^1, x^2, \ldots, x^\tau\}$ is the set of unstable structures that are feasible for problem (17), where $x^k \in \mathbb{R}^m$ for $k = 1, \ldots, \tau$ are the cross-sectional area vectors corresponding to each of the unstable structures. Let $\mathcal{E}_k$, for $k = 1, \ldots, \tau$, denote the event that structure x^k is infeasible for problem (17) with perturbed external force $\bar{f}$, and let $\mathcal{F}_k$ be the complement of $\mathcal{E}_k$, that is, $\mathcal{F}_k$ is the event that structure x^k is feasible for the perturbed version of problem (17). Next, we calculate the probability of the event that all the structures from set $\mathcal{X}$ are infeasible, that is, we compute $\Pr(\bigcap_{k=1}^{\tau} \mathcal{E}_k)$. Notice that

$$\bigcap_{k=1}^{\tau} \mathcal{E}_k = \left(\bigcup_{k=1}^{\tau} \mathcal{E}_k^c \right)^c = \left(\bigcup_{k=1}^{\tau} \mathcal{F}_k \right)^c.$$

From Lemma 1, it follows that $\Pr(\mathcal{F}_k) = 0$ for $k = 1, \ldots, \tau$. Thus, $\Pr(\bigcup_{k=1}^{\tau} \mathcal{F}_k) = 0$, or equivalently

$$\Pr\left(\bigcap_{k=1}^{\tau} \mathcal{E}_k \right) = 1.$$

Therefore, the probability that all the unstable structures are infeasible is one, i.e., the probability that the feasible set of the problem with perturbation (24) includes a kinematically unstable structure is zero. □ □

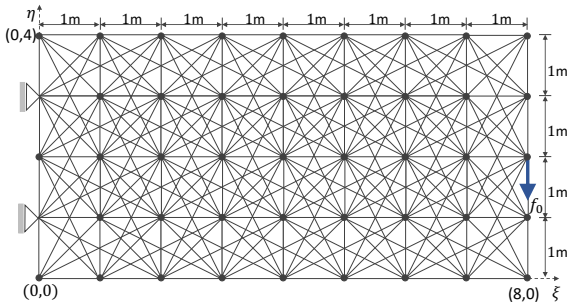

Figure 2: Michell truss ground structure 8-4-2-2 with 244 bars.

5 Computational experiments

In this section, we present our numerical results. A family of Michell truss structures (Sokół, 2011) serves as a test set library. First, we compare the optimization model (17) with and without random perturbation of the external forces to demonstrate the impact of the perturbation on the kinematic stability of the structure obtained from model (17). Moreover, we demonstrate the impact of adding necessary constraints (20) and (21) on the solution time of model (17). Finally, we compare the solution time and optimized weight obtained from model (17) with those of the model proposed by Mela (2014).

Computations are carried out on a desktop workstation with Dual Intel Xeon® CPU 2630 @ 2.20 GHz (20 cores) and 64 GB of RAM. Gurobi 9.0.0 (2019) is used to solve the MILO models. Gurobi has the capability of using multiple threads in solving a MILO problem with the branch and bound algorithm and is set to use 10 threads in solving the MILO models. Since Gurobi exhausts memory in solving the large MILO models, the `NodefileStart` parameter is set to 64 GB, which limits the memory to that amount. When the memory is at the limit, the nodes are compressed and written to a local disk. The maximum solution time is set to one day. Other Gurobi parameters remain at the default values.

5.1 Michell Structure

Michell trusses (Sokół, 2011), which are known scalable two-dimensional truss problems, are used to obtain the numerical results. A Michell truss is defined by four parameters: $n_\xi, n_\eta, d_\xi, d_\eta$. Parameters n_ξ and n_η stand for the number of blocks in the ξ and η directions, respectively, and n_η is a multiple of 4. Parameters d_ξ and d_η describe the connectivity of diagonal bars in the ground structure. A Michell truss has $(n_\xi + 1) \times (n_\eta + 1)$ nodes. Node (i, j), for $0 \leq i \leq n_\xi$ and $0 \leq j \leq n_\eta$, is connected to node (i', j') in the ground structure, if $i - d_\xi \leq i' \leq i + d_\xi$ and $j - d_\eta \leq j' \leq j + d_\eta$. It should be noted that, unlike the structure considered by Sokół (2011), we allow overlapping bars in the ground structure. Nodes $(0, n_\eta/4)$ and $(0, 3n_\eta/4)$ are fixed. A downward external force f_0 is exerted on node $(n_\xi, n_\eta/2)$. The ground structures of the Michell trusses are all kinematically stable. In Figure 2, the Michell ground structure 8-4-2-2 with its associated external force is illustrated.

The discrete set of candidate radii of the cross-sectional areas of the bars in the Michell truss is set to $\{2, 2.5, 3, 3.5, 4, \ldots, 8\}$ cm, and $\pi = 3.14$. In Table 1, the parameters of the Michell trusses are given. All the bars of the Michell trusses are assumed to be made from the same material. The data of the Michell trusses that are solved in this study are made publicly available[1].

Table 1: Parameters used in Michell trusses.

Property	Value
f_0	8×10^5 N
ρ	$2,768\,\mathrm{kg/m}^3$
E	69 GPa
$u^{\max}$	$2n_\xi$ cm
$u^{\min}$	$-2n_\xi$ cm
$\sigma^{\max}$	172.36 MPa
$\sigma^{\min}$	−172.36 MPa

In Table 2, the number of bars and the number of nodes of all the Michell trusses considered in this article are presented. It should be noted that model (17) has mv binary variables and $mv + dn + 5m$ continuous variables.

5.2 Effect of perturbation variance ϵ

We demonstrate how changing the magnitude of the variance of the random perturbations of the external forces, as introduced in Section 4.2, affects the optimal structure. In this numerical experiment we consider the Michell truss 3-4-2-2 and ϵ takes values from the set $\{0, 10^{-5}f_0, 10^{-4}f_0, 10^{-3}f_0, 10^{-2}f_0\}$. We draw 1000 random perturbations of the external forces for each of the non-zero values of ϵ, and thus, we solve 1000 optimization problems for each non-zero value of ϵ. Computers are able to compute with double precision floating point arithmetic. Therefore, we decrease the feasibility tolerance of the Gurobi solver, as ϵ gets smaller to avoid numerical issues. Note that the feasibility tolerance of Gurobi is dictated by parameters `FeasibilityTol` and `IntFeasTol`.

In Table 3, the percentage of the optimization problems leading to kinematically stable structures along with the range of the optimal weights and average solution time is reported for each value of ϵ. In this numerical experiment `FeasibilityTol` and `IntFeasTol` are both equal to the values of the "Feasibility Tolerance" column. From Table 3, we can see that, given the appropriate value of feasibility tolerance, the resulting structures are always stable for all the non-zero values of ϵ. The results listed in Table 3 computationally verify Theorem 1.

The parameter ϵ should be set so small that the resulting random perturbation does not change the characteristic of the external load. In our demonstration one observes

[1] https://github.com/shahabsafa/truss-data.git

[2] In the mathematical model implementation, m extra auxiliary continuous variables are used to represent the sum of the stress variables, $\sum_{k\in\mathcal{K}} \sigma_{ik}$, for $i = 1, \ldots, m$. The number of continuous variables, reported in the table, includes those m auxiliary variables.

Table 2: Michell trusses

Problem (n_ξ-n_η-d_ξ-d_η)	# nodes	# bars	# constrs.	# cont. vars.[2]	# binary vars.
1-4-1-1	10	21	1,041	394	273
2-4-1-1	15	38	1,896	710	494
2-4-2-2	15	78	4,258	1,430	1,014
2-4-2-4	15	105	6,370	1,916	1,365
3-4-1-1	20	55	2,751	1,026	715
3-4-2-2	20	123	6,920	2,250	1,599
3-4-3-3	20	174	11,501	3,168	2,262
3-4-3-4	20	190	12,993	3,456	2,470
4-4-1-1	25	72	3,606	1,342	936
4-4-2-2	25	168	9,588	3,070	2,184
4-4-3-3	25	252	17,894	4,582	3,276
4-4-4-4	25	300	25,111	5,446	3,900
5-4-1-1	30	89	4,461	1,658	1,157
5-4-2-2	30	213	12,256	3,890	2,769
5-4-3-3	30	330	24,403	5,996	4,290
5-4-4-4	30	410	38,084	7,436	5,330
5-4-5-4	30	435	43,365	7,886	5,655
6-4-6-4	35	595	70,832	10,776	7,735
7-4-7-4	40	780	110,086	14,116	10,140
8-4-8-4	45	990	164,654	17,906	12,870

Table 3: Effect of variance parameter ϵ on the optimal solution of the Michell truss 3-4-2-2.

ϵ	Feasibility Tolerance	# Problems	Kinematic Stability (%)	Opt. weight range (kg)	Avg. sol. time (s)
0	10^{-9}	1	0	152.69	18.09
$10^{-5}f_0$	10^{-9}	1000	100	[155.99–156.89]	33.54
$10^{-4}f_0$	10^{-8}	1000	100	155.99	32.94
$10^{-3}f_0$	10^{-7}	1000	100	155.99	32.85
$10^{-2}f_0$	10^{-6}	1000	100	[144.57–162.25]	40.26

that for the Michell truss 3-4-2-2, if $\epsilon = 10^{-2}f_0$, then it changes the optimal weight and also the optimal solution, since it significantly changes the external load structure.

Furthermore, it should be noted that changing the value of ϵ changes the coefficient matrix of the constraints. Choosing a too small value for ϵ can potentially lead to numerically ill-conditioned problems. As it can be seen for the cases where $\epsilon = 10^{-5}$, there is a slight variation in the total weight of the optimal structures due to numerical issues. To prevent numerical difficulties, we choose the largest possible perturbation which has no impact on the optimal solution.

From Table 3, we observe that ϵ can take a value in range $[10^{-4}f_0, 10^{-3}f_0]$ for the Michell truss 3-4-2-2 without changing the solution. We checked the acceptable range of ϵ for different Michell trusses. It turns out that $\epsilon = 10^{-3}f_0$ is appropriate for all the Michell trusses that are considered in this article.

5.3 Effects of necessary conditions and external force perturbation

Figures 3 through 5 illustrate the effects of bar-crossing elimination constraints (14) and (15), bar-overlapping elimination constraints (16), constraints (20) and (21) which are necessary for kinematic stability, and the external force perturbation (22) on

model (17). In all Figures 3, 4, and 5, sub-figure

(a) is the optimal solution of model (17) without bar-crossing elimination constraints (14) and (15) and bar-overlapping elimination constraints (16),

(b) is the optimal solution of model (17),

(c) is the optimal solution of model (17) with constraints (20) and (21) which are necessary for kinematic stability,

(d) is the optimal solution of model (17) with constraints (20) and (21) and the external force perturbation (22).

In Figures 3(a), 4(a), and 5(a), we have overlapping and crossing bars. For visualization, overlapping bars are slightly shifted in the figures. Figures 3(b), 4(b), and 5(b) demonstrate that the crossing bars and overlapping bars are eliminated by adding constraints (14), (15), and (16).

In Figure 3(b), we have four hinges at nodes (1,1), (2,1), (1,2), and (1,3). Adding constraints (20) and (21) to model (17), as Figure 3(c) demonstrates, eliminates all the hinge nodes. Hinge node (1,3) is eliminated by replacing two short bars with a long bar. The other three hinge nodes are eliminated by connecting extra bars to those nodes. We observe the same phenomena in Figures 4(b) and 5(b), and see in Figures 4(c) and 5(c) that all the hinges are eliminated by adding constraints (20) and (21), which are derived from Proposition 1. Constraints (20) and (21) are necessary for the kinematic stability of the structure; however, they are not sufficient to guarantee kinematic stability. For example, Michell structure 5-4-2-2 in Figure 4(c) becomes stable by adding necessary constraints (20) and (21). However, Michell structures 4-4-2-2 and 5-4-5-4 in Figures 3(c) and 5(c) are not kinematically stable after adding constraints (20) and (21).

As proved in Theorem 1, adding the external force perturbation (22) is sufficient to guarantee kinematic stability. In Figures 3(d), 4(d), and 5(d), the structures are kinematically stable due to the external force perturbation. Enforcing kinematic stability by adding the external force perturbation can lead to a significantly different truss topology compared to the structure obtained from solving the model without the external force perturbation. Michell truss 4-4-2-2 is an example where adding the external force perturbation results in a significantly different truss topology as can be seen in Figure 3(d) compared to Figure 3(b). Although structure 3(d) is topologically different from structure 3(b), the weight of structure 3(d) is only 3% higher than the one in Figure 3(b).

As proved in Theorem 1, adding the external force perturbation (24) to model (17) is sufficient to obtain a kinematically stable structure. Adding necessary constraints (20) and (21) to the proposed model, though, is useful in reducing the solution time. In Table 4, the impact of adding necessary constraints (20) and (21) on the solution time of the proposed model is demonstrated. In this table, "TL" stands for the cases where the 24-hour time limit passed without proving optimality. We can see in the table that adding the necessary constraints (20) and (21) can significantly reduce the solution time, e.g., up to 94% for the Michell truss 5-4-1-1.

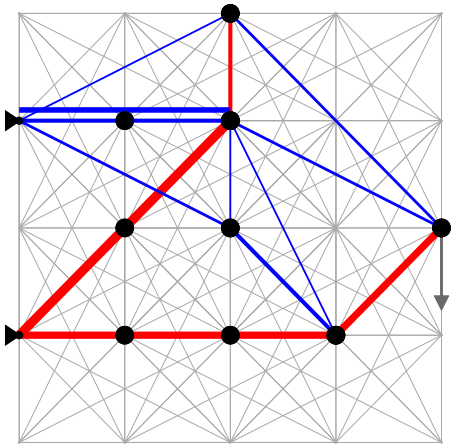

(a)) Model (17) without constraints (14), (15), and (16). The structure is **unstable**.

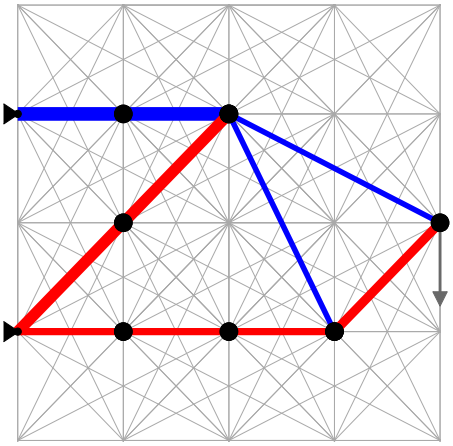

(b)) Model (17). The structure is **unstable**.

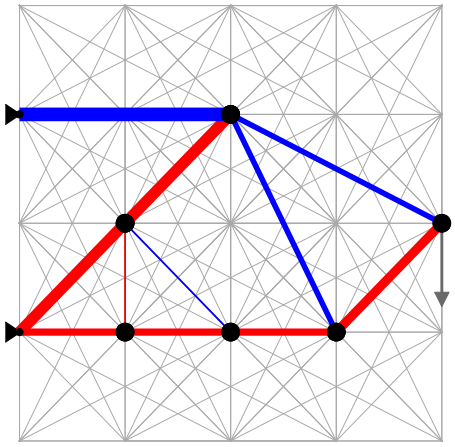

(c)) Model (17) with constraints (20) and (21). The structure is **unstable**.

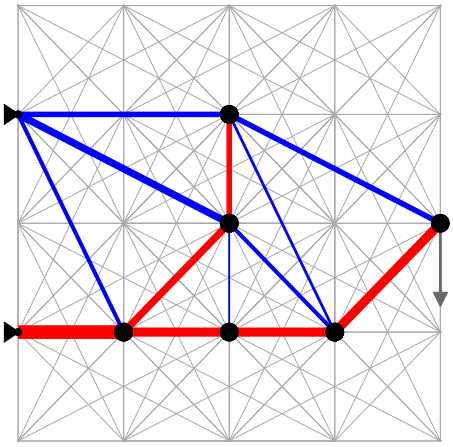

(d)) Model (17) with constraints (20) and (21) and perturbation (24). The structure is **stable**.

Figure 3: Optimal structures of the Michell truss 4-4-2-2.

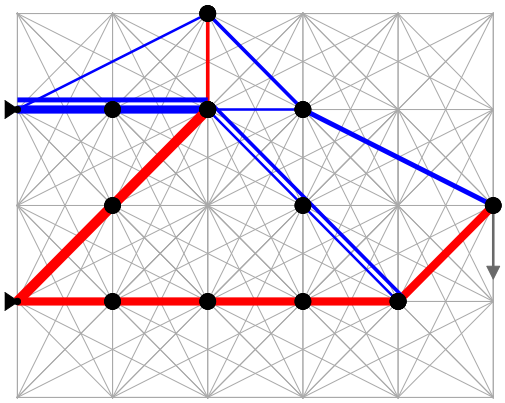

(a)) Model (17) without constraints (14), (15), and (16). The structure is **unstable**.

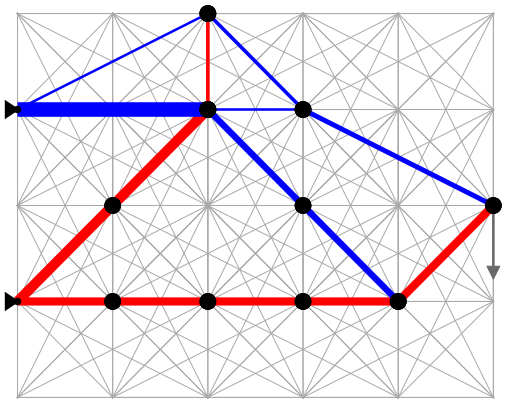

(b)) Model (17). The structure is **unstable**.

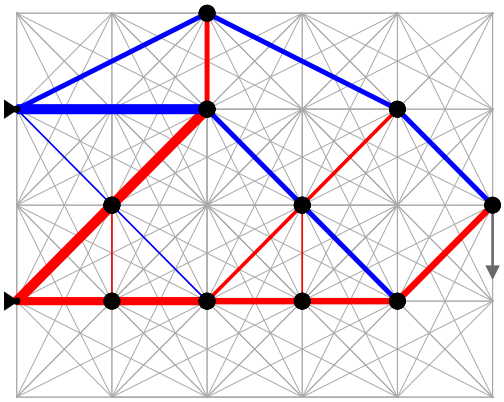

(c)) Model (17) with constraints (20) and (21). The structure is **stable**.

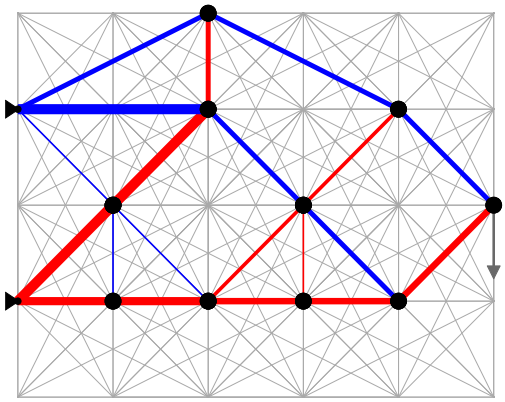

(d)) Model (17) with constraints (20) and (21) and perturbation (24). The structure is **stable**.

Figure 4: Optimal structures of the Michell truss 5-4-2-2.

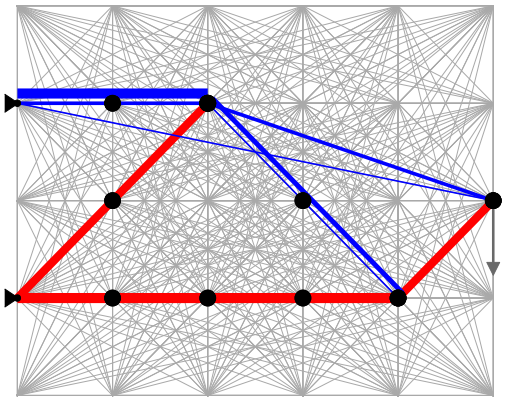

(a)) Model (17) without constraints (14), (15), and (16). The structure is **unstable**.

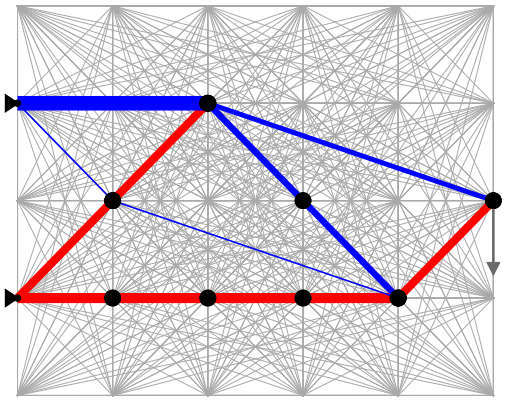

(b)) Model (17). The structure is **unstable**.

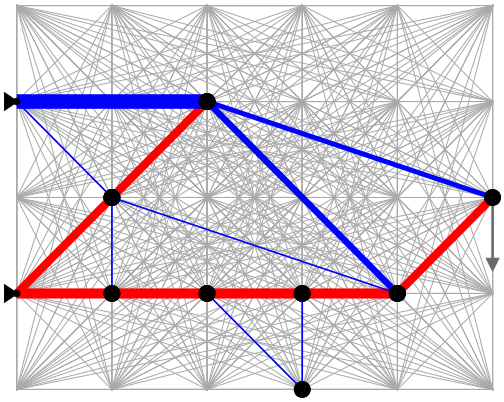

(c)) Model (17) with constraints (20) and (21). The structure is **unstable**.

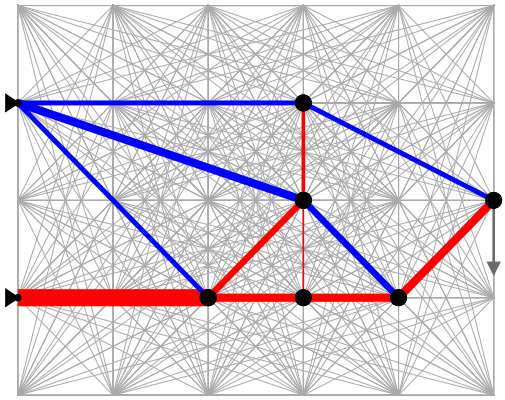

(d)) Model (17) with constraints (20) and (21) and perturbation (24). The structure is **stable**.

Figure 5: Optimal structures of the Michell truss 5-4-5-4.

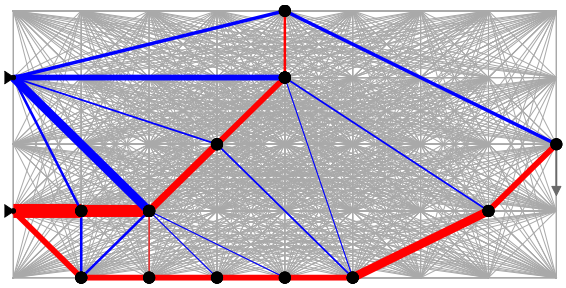

(a)) The structure plotted without the nodal displacements.

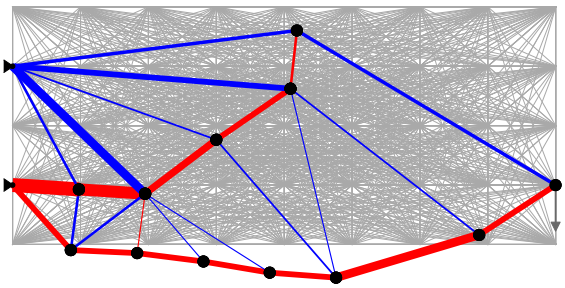

(b)) The structure plotted with the nodal displacements.

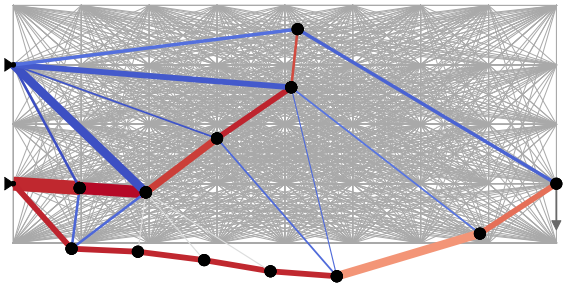

(c)) The distribution of stress in the final structure.

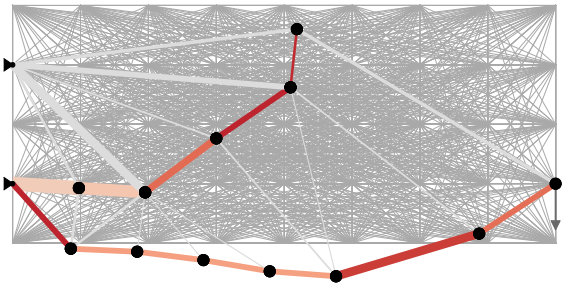

(d)) The distribution of Euler buckling in the final structure.

Figure 6: Solution obtained from model (17) with constraints (20) and (21) and external force perturbation (24) for Michell truss 8-4-8-4. For better visibility, the displacements are magnified by a factor of 10.

It can be seen from Table 4 that the optimal solutions of the Michell trusses 5-4-3-3, 5-4-4-4, and 5-4-5-4 are the same. However, the solution time increases in these three instances, as the feasible set of the problem gets larger.

Figure 6 shows the Michell truss 8-4-8-4 obtained by solving model (17) with constraints (20) and (21) and external force perturbation (24) using a 24-hour solution time budget. Figures 6(a) and 6(b) illustrate the optimal structures without and with nodal displacements, respectively. We, additionally, show the distribution of yield stress and Euler buckling stress in Figures 6(c) and 6(d), respectively.

5.4 Comparison of the proposed MILO model with Mela's model

In this section, we compare the optimization model (17), with constraints (20) and (21) added, with the model proposed by Mela (2014). In both models, perturbations of the external forces are considered, though perturbations in the two models are different. Mela (2014) used the external force perturbation proposed by Faustino et al. (2006).

Table 4: Optimized weights (kg), solution times (s), and memory usage (MB) for the proposed model with external force perturbation (24), and with and without constraints (20) and (21).

Problem	w/ perturbation (24) and w/o constrs. (20, 21)			w/ perturbation (24) and w/ constrs. (20, 21)		
	memory	weight	sol. time	memory	weight	sol. time
1-4-1-1	84	33.87	0.10	84	33.87	0.07
2-4-1-1	133	98.26	1.36	136	98.26	1.17
2-4-2-2	136	84.29	2.78	142	84.29	4.00
2-4-2-4	151	84.29	4.14	153	84.29	5.09
3-4-1-1	186	162.65	13.94	177	162.65	8.04
3-4-2-2	273	155.99	34.68	290	155.99	31.99
3-4-3-3	341	145.46	33.79	349	145.46	17.82
3-4-3-4	330	145.46	22.77	381	145.46	35.35
4-4-1-1	3,212	253.07	5,060.73	1,088	253.07	1,012.88
4-4-2-2	943	231.25	872.85	729	231.25	240.56
4-4-3-3	1,649	231.25	2166.33	1,125	231.25	592.86
4-4-4-4	1,223	227.73	599.03	1,178	227.73	230.68
5-4-1-1	32,419	339.76	TL	3,041	339.76	4,781.79
5-4-2-2	44,542	321.84	TL	6,187	321.84	11,065.10
5-4-3-3	19,427	317.69	54,037.36	4,450	317.69	9,047.89
5-4-4-4	17,948	314.30	49,808.39	4,561	317.69	12,139.52
5-4-5-4	49,802	318.96	TL	7,608	317.69	18,268.83
6-4-6-4	20,044	427.64	TL	28,718	422.98	TL
7-4-7-4	21,358	545.20	TL	23,743	539.68	TL
8-4-8-4	15,057	699.57	TL	19,740	657.12	TL

However, no guidelines were provided on how the random external force perturbations are generated. To get reasonable comparison, the distribution that is used to generate external force perturbations in our proposed model is also used for the external force perturbations in the model proposed by Mela (2014). To make the forces comparable, we set $\epsilon = 2 \times 10^{-3}$ in Mela's model, since force perturbations are tied to the active nodes as opposed to our model where force perturbations are tied to the active bars. The node-based perturbation in the model proposed by Mela (2014) is chosen two times the size of the bar-based perturbation since in a 2D kinematically stable truss, at least two bars are connected to each active pinned node. Parameters `FeasibilityTol` and `IntFeasTol` are set to their default values for both models and all the structures obtained are kinematically stable.

In Table 5, t and w denote the solution time and the weight of the structure obtained from the model proposed by Mela (2014), respectively; and t' and w' denote the solution time and the weight of the structure obtained from model (17), respectively. The optimality gap is the percentage of the gap between the lower and upper bounds of the optimal objective value w.r.t. the upper bound that is reported by Gurobi. Further, "TL" stands for the cases where the 24-hour time limit passed without proving optimality. If no feasible solution is found within the 24-hour time limit, the sign "—" is used in the optimality gap and weight columns.

Table 5 shows that for the large truss problems, the proposed model (17) can be solved significantly faster (e.g., more than nine times for the Michell truss 5-4-3-3 while the model proposed by Mela (2014) could not prove optimality), and the quality of solution is significantly better within the given time limit (e.g., the weight reported by the proposed model is 539.68 kg vs. 587.65 kg of the Mela's model for the Michell truss 7-4-7-4). One can observe that, as the size of the problem grows, the increase in the solution time of the model proposed by Mela (2014) is significantly higher than that of our proposed model. The model proposed by Mela (2014) fails to provide a feasible solution in the 24-hour time limit for the Michell truss 8-4-8-4; while our proposed model provides a high-quality solution in the same time limit.

6 Conclusions

In this paper, we developed a novel mixed integer linear optimization (MILO) model for the discrete truss topology design and sizing optimization (TTDSO) problem. We introduced necessary conditions that are required for a truss structure to be kinematically stable. Moreover, by introducing novel external force perturbations, we proved that the solutions of the MILO model are kinematically stable with probability one. We presented numerical results to demonstrate the efficacy and efficiency of the proposed MILO model with the external force perturbation in providing kinematically stable structures. Compared to the model proposed by Mela (2014), we demonstrated that our MILO model is up to 9 times faster in proving the global optimality of the Michell trusses. With the novel proposed model, we have obtained high-quality solutions for Michell trusses with up to 990 bars and considering 13 different cross-sectional areas in the ground structure.

Table 5: Optimality gaps (%), weights (kg) and the solution times (s) for our proposed model and the model proposed by Mela (2014).

Problem	Mela (2014)			The proposed model			t/t'
	opt. gap	w	t	opt. gap	w'	t'	
1-4-1-1	0.00	33.87	0.10	0.00	33.87	0.07	1.43
2-4-1-1	0.00	98.26	3.00	0.00	98.26	1.17	2.56
2-4-2-2	0.00	84.29	3.02	0.00	84.29	4.00	0.76
2-4-2-4	0.00	84.29	5.02	0.00	84.29	5.09	0.99
3-4-1-1	0.00	162.65	15.91	0.00	162.65	8.04	1.98
3-4-2-2	0.00	155.99	38.22	0.00	155.99	31.99	1.19
3-4-3-3	0.00	145.46	13.27	0.00	145.46	17.82	0.74
3-4-3-4	0.00	145.46	22.55	0.00	145.46	35.35	0.64
4-4-1-1	0.00	253.07	7,037.59	0.00	253.07	1,012.88	6.95
4-4-2-2	0.00	231.25	1,788.64	0.00	231.25	240.56	7.44
4-4-3-3	0.00	231.25	1,541.55	0.00	231.25	592.86	2.60
4-4-4-4	0.00	226.99	1,175.69	0.00	227.73	230.68	5.10
5-4-1-1	0.00	339.76	29,556.33	0.00	339.76	4,781.79	6.18
5-4-2-2	0.00	321.84	25,019.21	0.00	321.84	11,065.10	2.26
5-4-3-3	0.85	317.69	TL	0.00	317.69	9,047.89	> 9.55
5-4-4-4	2.09	317.69	TL	0.00	317.69	12,139.52	> 7.12
5-4-5-4	1.34	317.69	TL	0.00	317.69	18,268.83	> 4.73
6-4-6-4	6.09	423.99	TL	4.61	422.98	TL	NA
7-4-7-4	19.08	587.65	TL	8.42	539.68	TL	NA
8-4-8-4	—	—	TL	10.40	657.12	TL	NA

Standard MILO solvers are used in this paper to solve the TTDSO problems. Special purpose solution methodologies can be developed in the future to solve larger-scale TTDSO problems (Shahabsafa et al., 2018).

7 Replication of results

The data of the Michell trusses that are solved in this study are made publicly available in the GitHub repository: `https://github.com/shahabsafa/truss-data.git`. The repository, for each test problem, includes both the raw data of the structure and the MPS file used as input for the Gurobi solver.

In the computational experiments, we used the commercial, state-of-the-art, mixed integer linear optimization software Gurobi (2019) to solve all test problems. The specification of the workstation used, and the specific parameter settings of Gurobi ver. 9.0.0 solver are presented on page 16, at the beginning of Section 5.

Conflict of Interest

The authors declare that they have no conflict of interest.

Acknowledgment

This research was supported by Air Force Office of Scientific Research Grant #FA9550-15-1-0222. The authors would like to thank the editors and the referees to provide constructive suggestions which allowed us to improve the article significantly.

Appendix A

In the basic discrete model, the choice constraints for the TTDSO problem are defined as:

$$\begin{aligned} & x_i = \sum_{k\in\mathcal{K}} s_k z_{ik}, && i \in \mathcal{I}, \\ & \sum_{k\in\mathcal{K}} z_{ik} = y_i, && i \in \mathcal{I},\ k \in \mathcal{K}, \\ & y_i \in \{0,1\}, && i \in \mathcal{I}, \\ & z_{ik} \in \{0,1\}, && i \in \mathcal{I}, k \in \mathcal{K} \cup \{0\}. \end{aligned} \tag{26}$$

To enforce equalities (8) and (9), the following set of constraints is needed:

$$\begin{aligned} (1-y_i)\underline{\sigma}_i^{\mathrm{d}} \ \leq\ & \sigma_i^{\mathrm{d}} \ \leq\ (1-y_i)\overline{\sigma}_i^{\mathrm{d}}, && i \in \mathcal{I}, \\ \max\left(-\gamma_i s_k, \sigma_i^{\min}\right) z_{ik} \ \leq\ & \sigma_{ik} \ \leq\ \sigma_i^{\max} z_{ik}, && i \in \mathcal{I},\ k \in \mathcal{K}. \end{aligned} \tag{27}$$

The Euler buckling constraints are incorporated in the set of constraints (27) as well. The basic MILO model for TTDSO is defined as

$$
\begin{array}{lllll}
\min & \displaystyle\sum_{i\in\mathcal{I}} \rho l_i x_i, & & & \\
\text{s.t.} & Rq & = f, & & \\
& R^T u & = \Delta l, & & \\
& x_i - \displaystyle\sum_{k\in\mathcal{K}} s_k z_{ik} & = 0, & i \in \mathcal{I}, & \\
& \lambda_i \Delta l_i - \displaystyle\sum_{k\in\mathcal{K}} \sigma_{ik} - \sigma_i^{\mathrm{d}} & = 0, & i \in \mathcal{I}, & \\
& q_i - \displaystyle\sum_{k\in\mathcal{K}} s_k \sigma_{ik} & = 0, & i \in \mathcal{I}, & \\
& \displaystyle\sum_{k\in\mathcal{K}} z_{ik} & = y_i, & i \in \mathcal{I}, & \\
& \max\left(-\gamma_i s_k, \sigma_i^{\min}\right) z_{ik} & \le \sigma_{ik} \le \sigma_i^{\max} z_{ik} & i \in \mathcal{I},\ k \in \mathcal{K}, & \\
& u_\ell^{\min} & \le u_\ell \le u_\ell^{\max}, & \ell \in \mathcal{L}, & \\
& (1-y_i)\underline{\sigma}_i^{\mathrm{d}} & \le \sigma_i^{\mathrm{d}} \le (1-y_i)\overline{\sigma}_i^{\mathrm{d}}, & i \in \mathcal{I}, & \\
& y_{i_1} + y_{i_2} & \le 1, & (i_1, i_2) \in \mathcal{A}^{\mathrm{p}}, & \\
& \displaystyle\sum_{\bar{i}\in\mathcal{A}_i} y_{\bar{i}} & \le |\mathcal{A}_i|(1-y_i), & i \in \mathcal{I}, & \\
& \displaystyle\sum_{\bar{i}\in\mathcal{C}_i} y_{\bar{i}} & \le 1, & i \in \mathcal{I}^B, & \\
& y_i \in \{0,1\}, & i \in \mathcal{I}, & & \\
& z_{ik} \in \{0,1\}, & i \in \mathcal{I},\ k \in \mathcal{K}. & &
\end{array}
\tag{28}
$$

If $y_i = 1$, for $i \in \mathcal{I}$, then the problem reduces to a truss sizing optimization problem. In a truss sizing optimization problem, bar-crossing elimination and bar-overlapping elimination constraints are not needed, since the topology of the structure is predetermined by the ground structure.

Appendix B

The list of the definitions of the article is given in Table 6.

Table 6: List of definitions.

No.	Page	Definition
1	8	Overlapping set
2	8	Maximal overlapping set
3	8	Base element of a maximal overlapping set
4	10	Active bars
5	10	Active nodes
6	10	Active coordinates
7	10	Reduced topology matrix
8	10	Reduced stiffness matrix
9	11	Kinematic stability
10	11	Orientation vector
11	12	Maximal non-spanning set

The decision variables of the mathematical model and the parameters introduced in the article are presented in Tables 7 and 8, respectively.

Table 7: List of the decision variables of the mathematical models.

Variable	Definition
x_i	The cross-sectional area of bar i
y_i	$\begin{cases} 1, & \text{if } x_i > 0, \\ 0, & \text{otherwise.} \end{cases}$
z_{ik}	$\begin{cases} 1, & \text{if } x_i > s_k, \\ 0, & \text{otherwise.} \end{cases}$
u	The the displacement vector of the pinned nodes
Δl_i	The elongation of bar i
σ_{ik}	The stress on bar i if $x_i = s_k$
q_i	The internal force of bar i
σ_i^{d}	$\begin{cases} \lambda_i \Delta l_i, & \text{if } x_i = 0, \\ 0, & \text{otherwise.} \end{cases}$
p	The vector of the random perturbations
$\bar{f}$	The perturbed external force

References

Aage, N., Andreassen, E., Lazarov, B. S., and Sigmund, O. (2017). Giga-voxel computational morphogenesis for structural design. *Nature*, 550(7674):84–86.

Achtziger, W. and Kočvara, M. (2007). On the maximization of the fundamental eigenvalue in topology optimization. *Structural and Multidisciplinary Optimization*, 34(3):181–195.

Arora, J. and Wang, Q. (2005). Review of formulations for structural and mechanical system optimization. *Structural and Multidisciplinary Optimization*, 30(4):251–272.

Ben-Tal, A. and Bendsøe, M. P. (1993). A new method for optimal truss topology design. *SIAM Journal on Optimization*, 3(2):322–358.

Bendsøe, M. P. (1989). Optimal shape design as a material distribution problem. *Structural Optimization*, 1(4):193–202.

Bendsøe, M. P., Ben-Tal, A., and Zowe, J. (1994). Optimization methods for truss geometry and topology design. *Structural Optimization*, 7(3):141–159.

Bons, N. P. and Martins, J. R. R. A. (2020). Aerostructural wing design exploration with multidisciplinary design optimization. In *AIAA Scitech 2020 Forum*, Orlando, Florida, 6-10 January.

Brooks, T. R., Kenway, G. K. W., and Martins, J. R. R. A. (2017). Undeflected common research model (uCRM): An aerostructural model for the study of flexible transonic aircraft wings. In *35th AIAA Applied Aerodynamics Conference*, AIAA paper 2017-4456, Denver, Colorado, 5-9 June.

Chauhan, S. S. and Martins, J. R. R. A. (2018). Low-fidelity aerostructural optimization of aircraft wings with a simplified wingbox model using OpenAeroStruct. In *Proceedings of the 6th International Conference on Engineering Optimization, EngOpt 2018*, pages 418–431, Lisbon, Portugal. Springer.

Dorn, W. S., Gomory, R. E., and Greenberg, H. J. (1964). Automatic design of optimal structures. *Journal de Mecanique*, 3:25–52.

Faustino, A. M., Júdice, J. J., Ribeiro, I. M., and Neves, A. S. (2006). An integer programming model for truss topology optimization. *Investigação Operacional*, 26(1):11–127.

Gally, T., Pfetsch, M. E., and Ulbrich, S. (2018). A framework for solving mixed-integer semidefinite programs. *Optimization Methods and Software*, 33(3):594–632.

Ghosh, A. and Mallik, A. K. (2002). *Theory of Mechanisms and Machines*. Affiliated East-West Press Private Limited.

Gurobi Optimization Inc. (2019). Gurobi optimizer reference manual.

Haftka, R. T. and Gürdal, Z. (2012). *Elements of Structural Optimization*. Springer Science & Business Media.

Hajela, P. and Lin, C. Y. (1992). Genetic search strategies in multicriterion optimal design. *Structural Optimization*, 4(2):99–107.

Hashimoto, D. and Kanno, Y. (2015). A semidefinite programming approach to robust truss topology optimization under uncertainty in locations of nodes. *Structural and Multidisciplinary Optimization*, 51(2):439–461.

Jasa, J. P., Hwang, J. T., and Martins, J. R. R. A. (2018). Open-source coupled aerostructural optimization using Python. *Structural and Multidisciplinary Optimization*, 57(4):1815–1827.

Kanno, Y. (2016). Global optimization of trusses with constraints on number of different cross-sections: a mixed-integer second-order cone programming approach. *Computational Optimization and Applications*, 63(1):203–236.

Kanno, Y. (2018). Robust truss topology optimization via semidefinite programming with complementarity constraints: a difference-of-convex programming approach. *Computational Optimization and Applications*, pages 1–31.

Kanno, Y. and Fujita, S. (2018). Alternating direction method of multipliers for truss topology optimization with limited number of nodes: A cardinality-constrained second-order cone programming approach. *Optimization and Engineering*, 19(2):327–358.

Kanno, Y. and Guo, X. (2010). A mixed integer programming for robust truss topology optimization with stress constraints. *International Journal for Numerical Methods in Engineering*, 83(13):1675–1699.

Kennedy, G. J. (2016). A full-space barrier method for stress-constrained discrete material design optimization. *Structural and Multidisciplinary Optimization*, 54(3):619–639.

Kennedy, G. J. and Martins, J. R. R. A. (2014). A parallel aerostructural optimization framework for aircraft design studies. *Structural and Multidisciplinary Optimization*, 50(6):1079–1101.

Mela, K. (2014). Resolving issues with member buckling in truss topology optimization using a mixed variable approach. *Structural and Multidisciplinary Optimization*, 50(6):1037–1049.

Ohsaki, M. and Katoh, N. (2005). Topology optimization of trusses with stress and local constraints on nodal stability and member intersection. *Structural and Multidisciplinary Optimization*, 29(3):190–197.

Rajasekaran, S. and Sankarasubramanian, G. (2001). *Computational Structural Mechanics*. PHI Learning Pvt.

Rozvany, G. I. (2009). A critical review of established methods of structural topology optimization. *Structural and Multidisciplinary Optimization*, 37(3):217–237.

Rozvany, G. I. N. (1996). Difficulties in truss topology optimization with stress, local buckling and system stability constraints. *Structural Optimization*, 11(3):213–217.

Shahabsafa, M., Mohammad-Nezhad, A., Terlaky, T., Zuluaga, L., He, S., Hwang, J. T., and Martins, J. R. (2018). A novel approach to discrete truss design problems using mixed integer neighborhood search. *Structural and Multidisciplinary Optimization*, 58(6):2411–2429.

Sokół, T. (2011). A 99 line code for discretized michell truss optimization written in mathematica. *Structural and Multidisciplinary Optimization*, 43(2):181–190.

Stolpe, M. (2004). Global optimization of minimum weight truss topology problems with stress, displacement, and local buckling constraints using branch-and-bound. *International Journal for Numerical Methods in Engineering*, 61(8):1270–1309.

Stolpe, M. (2007). On the reformulation of topology optimization problems as linear or convex quadratic mixed 0–1 programs. *Optimization and Engineering*, 8(2):163–192.

Stolpe, M. (2015). Truss topology optimization with discrete design variables by outer approximation. *Journal of Global Optimization*, 61(1):139–163.

Stolpe, M. (2016). Truss optimization with discrete design variables: a critical review. *Structural and Multidisciplinary Optimization*, 53(2):349–374.

Stolpe, M. and Svanberg, K. (2004). A stress-constrained truss-topology and material-selection problem that can be solved by linear programming. *Structural and Multidisciplinary Optimization*, 27(1):126–129.

Sved, G. and Ginos, Z. (1968). Structural optimization under multiple loading. *International Journal of Mechanical Sciences*, 10(10):803 – 805.

Van Mellaert, R., Lombaert, G., and Schevenels, M. (2015). Global size optimization of statically determinate trusses considering displacement, member, and joint constraints. *Journal of Structural Engineering*, 142(2):04015120.

Zegard, T. and Paulino, G. H. (2014). GRAND – ground structure based topology optimization for arbitrary 2D domains using MATLAB. *Structural and Multidisciplinary Optimization*, 50(5):861–882.

Zegard, T. and Paulino, G. H. (2015). GRAND3 – ground structure based topology optimization for arbitrary 3D domains using MATLAB. *Structural and Multidisciplinary Optimization*, 52(6):1161–1184.

Zhou, M. and Rozvany, G. (1991). The COC algorithm, part II: Topological, geometrical and generalized shape optimization. *Computer Methods in Applied Mechanics and Engineering*, 89(1):309 – 336.

Zienkiewicz, O. C. and Taylor, R. L. (2005). *The Finite Element Method for Solid and Structural Mechanics*. Elsevier.

Table 8: List of the parameters of the article.

Parameter	Definition
d	The dimension of the space
m	The number of the bars of the ground structure
n	The degrees of freedom of the ground structure
v	The cardinality of the discrete set of cross-sectional areas
$\mathcal{I}$	The index set of the bars of the ground structure
$\mathcal{J}$	The index set of the pinned nodes of the ground structure
$\mathcal{S}$	The set of candidate non-zero cross-sectional areas of bars
$\mathcal{K}$	The set of indices corresponding to the discrete set $\mathcal{S}$
$\bar{\mathcal{K}}$	$\mathcal{K} \setminus \{v\}$
$\mathcal{L}$	The index set of the coordinates of the pinned nodes
$\mathcal{A}^{\mathrm{p}}$	The collection of pairs of bars that cross each other
$\mathcal{A}_i$	The set of bars that cross bar i
$\mathcal{I}^B$	The index set of all the base elements of the overlapping sets
$\mathcal{C}^B$	The maximal overlapping set corresponding to base element i
$\mathcal{N}_\ell$	The set of the bars of the ground structure that are connected to the node corresponding to the l-th coordinate of the displacement vector
$\mathcal{B}_j$	The set of bar indices connected to node j in the ground structure
$\mathcal{Q}_j$	The set of all the maximal non-spannig sets corresponding to node j that have at least a cardinality of d
R	The topology matrix of the ground structure
r_i	The i-th column of the topology matrix R
f	The vector of the external forces
E, E_i	The Young's modulus
ρ	The density of the truss material
l_i	The length of bar i
λ_i	$= E_i/l_i$
γ_i	$= \pi E_i/4l_i^2$
s_k	The k-th value of the discrete set of the cross-sectional areas
δ_k	$s_{k+1} - s_k$
$\sigma_i^{\min}, \sigma_i^{\max}$	The lower and upper bounds on the stress of bar i
$\underline{\sigma}_i^{\mathrm{d}}, \overline{\sigma}_i^{\mathrm{d}}$	The lower and upper bounds on the dummy variable σ^{d}
$u_\ell^{\min}, u_\ell^{\max}$	The lower and upper bounds on the ℓ-th coordinate of the nodal displacement vector